

# Investigating Anthropometric Fidelity in SAM 3D Body

Aizierjiang Aiersilan, Ruting Cheng, James Hahn  
 Institute for Innovation in Health Computing  
 The George Washington University  
 {alexandera, rcheng77, hahn}@gwu.edu

## Abstract

The recent release of SAM 3D Body [YKP<sup>+</sup>25] marks a significant milestone in human mesh recovery, demonstrating state-of-the-art performance in producing clean, topologically coherent meshes from single images. By leveraging the novel Momentum Human Rig (MHR), it achieves remarkable robustness to occlusion and diverse poses. However, our evaluation reveals a specific and consistent limitation: the model struggles to reconstruct detailed anthropometric deviations, especially on populations with special body shape alters such as geriatric muscle atrophy, scoliosis, or pregnancy, even when these features are prominent in the input image. In this paper, we investigate this phenomenon not as a failure of the model’s capacity, but as a byproduct of the *perception-distortion trade-off*. We posit that the architectural reliance on the low-dimensional parametric MHR representation, combined with semantic-invariant conditioning (DINOv3) and annotation-based alignment, creates a “regression to the mean” effect. We analyze these mechanisms to understand why individual biological details are smoothed out and propose specific, constructive pathways for future work to extend the impressive baseline performance of SAM 3D Body into the medical domain.

## 1 Introduction

3D foundation models (1) have historically trended toward universality, among which SAM 3D Body [YKP<sup>+</sup>25] continues this trend by effectively solving the “2D-to-3D lifting” problem for human subjects. Its capacity for human body generation not only facilitates human pose learning and unlocks new capabilities in robotics and interactive mixed reality applications, but also paves a promising road toward 3D body shape analysis in the medical domain. Recent clinical research has established that high-fidelity 3D anthropometry serves as a superior digital biomarker compared to traditional metrics like BMI, enabling early detection of metabolic risks, cardiovascular pathologies, and hormonal irregularities through precise morphological analysis [TCB<sup>+</sup>20, EHK24, GLMS<sup>+</sup>23, NSW<sup>+</sup>19]. Unlike its sibling model SAM 3D Objects [TCC<sup>+</sup>25], which targets general rigid objects, SAM 3D Body employs a specialized encoder-decoder architecture based on the Momentum Human Rig (MHR) [FOB<sup>+</sup>25] to decouple skeletal structure from surface shape, achieving a level of robustness that previous methods [XLX<sup>+</sup>25, ZLL<sup>+</sup>25] struggled to match.

However, the transition from general-purpose computer vision to medical application requires a shift in evaluation criteria—from perceptual plausibility to metric fidelity. Despite its capabilities, our internal testing uncovered a curious limitation. When tasked with reconstructing human bodies exhibiting specific medical or physiological conditions (e.g., third-trimester pregnancy, scoliosis, unilateral limb amputation, etc.), as shown in Figure 1, the model consistently produced “standardized” body shapes. Not only were textures like skin wrinkles and clothing smoothed out, but the overall geometry was also rectified to a generic mean. The typical scoliosis shape of the spine’s sideways curve and the abdominal region of the pregnant population were neglected during 3D figure generation. Driven by these observations, we investigate why

Table 1: An overview of recent 3D foundation models, landscape bifurcates into generative models (creating assets from text/images) and geometric understanding models (reconstructing scenes and motion).

Model	Primary Task	Example Applications	Key Features
<i>Generative 3D Models (Text/Image → 3D Asset)</i>			
SAM 3D Objects [TCC <sup>+</sup> 25]	Single-Image to Mesh	Robotics, AR/VR	Scalable synthetic training; occluded object recovery
SAM 3D Body [YKP <sup>+</sup> 25]	Human Mesh Recovery	Sports, Medical Analysis	Momentum Human Rig (MHR); decoupled skeleton/shape
TRELLIS [XLX <sup>+</sup> 25]	Text/Image to 3D	Game Dev, VFX	Structured Latent (SLAT); multi-format decode
Hunyuan3D 2.0 [ZLL <sup>+</sup> 25]	High-Fidelity Generation	AAA Gaming, Retail	Sparse-view DiT; PBR textures
MeshLLM [FSW <sup>+</sup> 25]	Text to Mesh	CAD, Design	LLM-based mesh tokens; editable topology
CAT3D [GHH <sup>+</sup> 24]	Multi-View Generation	Photorealistic Rendering	Diffusion-based NVS; high consistency
LGM [TCC <sup>+</sup> 24]	Fast Reconstruction	Real-time Previews	Large Geometry Model; asymmetric U-Net; outputs mesh or 3D Gaussians
SF3D [BHVJ25]	Textured Mesh Generation	E-commerce	UV-unwrapping; illumination disentanglement
AssetGen 2.0 [SMK <sup>+</sup> 24]	Text/Image to 3D Asset	Content Creation, Gaming	Single-stage 3D diffusion; improved view consistency; optional TextureGen module
Deep CAD [WXZ21]	Generative CAD Geometry	AEC, Manufacturing, Design	Precision CAD generation; trained on prod design data; design autocompletion
DreamFusion [PJBMM22]	Text-to-3D (NeRF)	Concept Art, Prototyping	Score Distillation Sampling (SDS); uses 2D diffusion models for 3D generation
<i>Geometric &amp; Scene Understanding (Structure / Motion)</i>			
DUS3R [WLC <sup>+</sup> 24]	Stereo Reconstruction	3D Scanning	Dense unconstrained stereo; pose-free camera estimation
MASt3R [LCR24]	3D Matching & Metric Rec.	Visual Localization, SfM	Pixel-wise 3D correspondences; metric pointmaps; cross-screen matching
MonST3R [ZHH <sup>+</sup> 25]	Dynamic Reconstruction (4D)	Autonomous Driving, Motion Capture	Extends DUS3R/MASt3R to dynamics; 4D pointmaps; no pose supervision
LoRA3D [LYX <sup>+</sup> 24]	Foundation Adaptation	Scene Fine-tuning	Low-rank self-calibration for geometric foundation models
MUSt3R [CSA <sup>+</sup> 25]	Multi-View Reconstruction	Visual Odometry, Mapping	Multi-view aggregation; global alignment-free; metric 3D output
PanSt3R [ZCM <sup>+</sup> 25]	3D Panoptic Segmentation	Robotics, Scene Analysis	Joint 3D geometry and panoptic segmentation; multi-view consistent
Copilot4D [ZXY <sup>+</sup> 24]	4D (3D + Time) Forecasting	Autonomous Driving	LiDAR tokenization; future state prediction; agent-conditioned forecasting

a model capable of reconstructing complex poses paradoxically struggles with organic biological variance. We argue that this behavior is a feature, rather than a bug, of current alignment strategies [CLB<sup>+</sup>17], and explore its critical implications for medical simulation. This work serves as a conceptual critique and a roadmap for bridging the gap between artistic generation and clinical reconstruction.

## 2 Related Work

### 2.1 Parametric Human Models and Phenotypic Diversity

The field of 3D human body modeling has long been dominated by SMPL [LMR<sup>+</sup>15] and its variants. While revolutionary, SMPL’s global shape space often suffers from spurious long-range correlations. To address this, STAR [OBB20] introduced sparse, spatially-local blend shapes, and SUPR [OBTB22] further refined this with a unified part-based representation to allow for more localized control. Most recently, AnnyBody [BFBS<sup>+</sup>25] has challenged the limited phenotypic range of standard models by explicitly modeling a diverse range of body shapes and medically meaningful morphs, highlighting the “standardization” bias inherent in older datasets. SAM 3D Body’s MHR, while robust, appears to regress to a similar global mean as early SMPL models, lacking the localized expressivity of SUPR or the population inclusivity of AnnyBody.

### 2.2 High-Fidelity and Implicit Reconstruction

To capture details beyond the parametric mesh, recent approaches have diverged from pure regression. HiLo [YLZ<sup>+</sup>24] explicitly separates high-frequency details (clothing, wrinkles) from low-frequency shape, ensuring that fine-grained geometry is not smoothed out. Similarly, CHROME [DZG<sup>+</sup>25] focuses on occlusion resilience and view consistency without over-relying on smooth priors. Implicit function approaches like SelfPIFu [XDW<sup>+</sup>24] abandon the mesh template entirely to learn topology-agnostic representations from in-the-wild data. In contrast, SAM 3D Body’s reliance on a fixed topology and low-dimensional MHR latent space inherently limits its ability to represent the high-frequency anomalies critical for medical diagnosis.

### 2.3 Biomechanical Fidelity

Beyond surface shape, the underlying skeletal accuracy is crucial. HSMR [XZV<sup>+</sup>25] integrates a biomechanically accurate skeleton into the reconstruction pipeline to prevent biologically implausible joint locations. While SAM 3D Body decouples skeleton and shape for robustness,



Figure 1: The limitations of SAM 3D Body when generating 3D figures for pregnant women (left, under license from Pressmaster - stock.adobe.com), people with scoliosis [Ton25] (middle left), people with limb loss (middle right, under license from Kawee - stock.adobe.com), and obese people (right, under license from DenisProduction.com - stock.adobe.com). Missing biological signature of each population is marked by a red box.

our analysis suggests it prioritizes pose plausibility over the metric accuracy required for biomechanical analysis, often “correcting” pathological skeletal deviations (e.g., scoliosis) to a healthy mean.

### 3 The Architectural Smoothing of Biology

#### 3.1 The Parametric Bottleneck of MHR

While general object reconstruction models like SAM 3D Objects [TCC<sup>+</sup>25] often suffer from the Nyquist limit of coarse voxelization ( $64^3$ ), SAM 3D Body avoids this by using the MHR. MHR is a parametric mesh representation that decouples skeletal structure from surface shape. While this decoupling is crucial for pose robustness, it imposes a *parametric bottleneck*.

The MHR model is defined by a shape vector  $\beta \in \mathbb{R}^{45}$  (comprising 20 body, 20 head, and 5 hand components), a skeleton transformation vector  $\gamma \in \mathbb{R}^{68}$ , and a facial expression vector  $\psi \in \mathbb{R}^{72}$ .

$$M(\beta, \gamma, \psi, \theta) = W(\bar{M} + B_s(\beta) + B_f(\psi) + B_p(\theta), S(\gamma), \theta) \quad (1)$$

where  $\bar{M}$  is the mean template,  $B_s$  and  $B_f$  are shape and expression blend shapes,  $B_p$  are pose correctives, and  $S(\gamma)$  represents the explicit skeleton parameterization.

It is particularly revealing to contrast this with the model’s treatment of extremities. Analysis of the MHR configuration reveals that the architecture allocates 72 components for face expression and 68 for skeletal proportions, yet compresses the core body morphology into just 20 components (within the 45-dimensional shape space). This allocation bias inherently favors facial expression and skeletal scaling over soft-tissue body morphology. Figure 2 illustrates this challenge by comparing body shapes captured by a commercial scanner (Fit3D, San Francisco, CA) with those reconstructed by SAM 3D body for both pregnant and non-pregnant women (the data collection was approved by the Institutional Review Board with number NCR224227, and informed consent was obtained from participants). The considerable morphological differences between these body types, which SAM 3D body can represent, must be compressed into MHR’s 45-component body basis. Consequently, anatomical features defining specific conditions (such

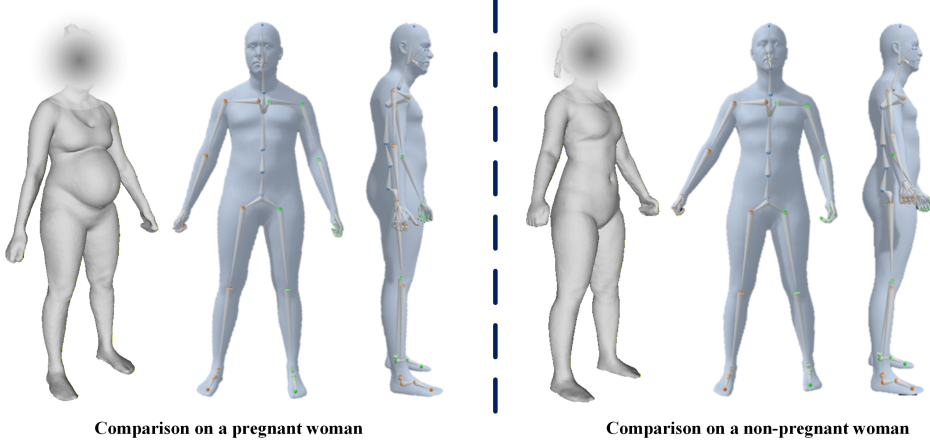


Figure 2: Comparison between body shapes obtained by commercial scanner and SAM 3D body on both pregnant woman and non-pregnant woman. The 3D figures generated by SAM 3D body are projected from front and side on the right of the scanner captured ones.

as the localized curvature of a postpartum abdomen or the spinal asymmetry of scoliosis) often lie outside the span of the learned body basis functions  $B_s$ . The model is structurally incapable of representing geometries that are orthogonal to its learned basis, forcing a projection onto the nearest “standard” shape regardless of the input evidence.

### 3.2 Semantic Invariance in DINOv3 Conditioning

SAM 3D Body conditions its geometry generation on features extracted by DINOv3 [SVS<sup>+</sup>25] (an evolution of DINOv2 [ODM<sup>+</sup>23]), a discriminative model trained to maximize semantic similarity and designed to be *invariant* to nuisance variables. It conceptually learns that a “person” is a “person” regardless of lighting, pose, or minor shape deformations. Formally, given an input image  $I$ , DINOv3 produces an embedding  $\mathbf{z} = f_{\text{DINO}}(I) \in \mathbb{R}^d$  where the encoder  $f_{\text{DINO}}$  is trained to minimize the distance between semantically similar images while remaining invariant to transformations  $\mathcal{T}$ :

$$\mathcal{L}_{\text{DINO}} = \mathbb{E}_{I, \mathcal{T}} [\|f_{\text{DINO}}(I) - f_{\text{DINO}}(\mathcal{T}(I))\|_2^2] \quad (2)$$

Furthermore, the backbone typically operates with a patch size of  $14 \times 14$  pixels (ViT-B/14), which inherently quantizes the spatial resolution of the input. We hypothesize that this spatial aggregation acts as a low-pass filter, effectively discarding high-frequency geometric cues such as skin folds or subtle protrusions before they even reach the decoder. While effective for general semantic recognition, this tokenization likely contributes to the loss of fine-grained medical details.

The architecture implicitly acknowledges this resolution limit for hands by employing a dedicated “zoom-in” inference strategy, where hand crops are re-processed at higher resolution via a separate decoder. Crucially, no such mechanism exists for the torso or spine. Consequently, the subtle texture cues of a surgical scar or the geometric cues of a protruding mass are lost in the global patch tokenization.

However, for medical reconstruction, these “minor deformations” are often the target signal. We hypothesize that the embeddings for “pregnant woman” and “woman” in DINOv3 are proximally located, causing the conditional generation network to default to the centroid of the “human” cluster. Let  $\mathbf{z}_{\text{std}}$  and  $\mathbf{z}_{\text{preg}}$  denote the embeddings for a standard woman and a pregnant woman, respectively. The semantic collapse manifests as:

$$\|\mathbf{z}_{\text{std}} - \mathbf{z}_{\text{preg}}\|_2 \ll \|\mathbf{g}_{\text{std}} - \mathbf{g}_{\text{preg}}\|_{\text{geo}} \quad (3)$$

where  $\mathbf{g}_{\text{std}}, \mathbf{g}_{\text{preg}}$  represent the true geometric representations. This phenomenon, known as *semantic collapse*, prioritizes the class label over metric fidelity [BM18]. Consequently, the conditional generation process  $p(M|\mathbf{z})$  regresses toward the empirical mean geometry  $\bar{M}_{\text{human}}$  of the training distribution.

## 4 The Alignment Tax: Why “Better” Means “Generic”

### 4.1 Dataset Bias in SAM 3D Body Dataset

While the real world naturally follows long-tail distributions, the training curricula for SAM 3D Body, specifically the SAM 3D Body Dataset [YKP<sup>+</sup>25], are constrained by the limitations of available high-quality 3D annotations. Let  $\mathcal{D}_{\text{real}}$  denote the natural distribution of human body geometries, modeled by a power-law tail. In contrast, the empirical training distribution  $\mathcal{D}_{\text{train}}$  is well-approximated by a truncated normal centered around “healthy” or “standard” subjects. The mismatch between these distributions can be formalized via the Jensen–Shannon divergence:

$$D_{\text{JS}}(\mathcal{D}_{\text{real}}, \mathcal{D}_{\text{train}}) = \frac{1}{2}D_{\text{KL}}(\mathcal{D}_{\text{real}}\|\mathcal{M}) + \frac{1}{2}D_{\text{KL}}(\mathcal{D}_{\text{train}}\|\mathcal{M}),$$

indicating that the model’s learned geometric prior is inevitably pulled toward the modes of  $\mathcal{D}_{\text{train}}$ .

The dataset construction involves a “multi-stage annotation pipeline” [YKP<sup>+</sup>25]. While this ensures high-quality pose labels, it likely introduces bias against morphological outliers:

**1) Annotation Bias and Idealized Forms.** Annotators or automated pseudo-labeling systems often rely on standard parametric fits (like SMPL) as a starting point. If the initial fit fails to capture a limb difference or a tumor, the final annotation will likely smooth it out. Thus, the dataset’s mass is concentrated near a narrow region of shape space. As the model estimates parameters via maximum likelihood over  $\mathcal{D}_{\text{train}}$ , its MAP reconstruction

$$\hat{G}_{\theta}(I) = \arg \max_{G'} p_{\theta}(G' | I)$$

is biased toward this limited region, systematically underrepresenting rare or extreme anatomical geometries [LMR<sup>+</sup>15].

**2) Missing High-Frequency Biological Detail.** The model has likely never encountered medical-grade meshes (e.g., CT/MRI reconstructions) containing high-frequency anatomical structures. Since meshes with high-frequency biological variance are absent in  $\mathcal{D}_{\text{train}}$ , SAM 3D Body lacks priors for shapes such as pregnancy-related deformation, pathological morphology, or age-related soft-tissue variation.

### 4.2 The Annotation Alignment Trap

A core strength of SAM 3D Body is its robust alignment, achieved through a data engine and multi-stage annotation. However, we argue this cycle is virtuous for robustness but detrimental for medical anomaly, interpreting medical cases as errors rather than valid variations. In a “human-in-the-loop” or “model-in-the-loop” annotation process, outliers are often flagged as errors. An annotator, presented with a noisy, lumpy mesh (which might accurately reflect a geriatric body) versus a smooth, clean mesh (generic body), will almost invariably select or correct towards the smooth one. This teaches the model a *smoothness prior*, a common regularization strategy in 3D reconstruction [PFS<sup>+</sup>19, MON<sup>+</sup>19], that actively penalizes biological

irregularities, treating them as artifacts to be corrected. Concretely, the learned policy implicitly minimizes a regularization term of the form:

$$\mathcal{R}_{\text{smooth}}(M) = \int_{\partial M} \|\nabla_s \mathbf{n}(\mathbf{p})\|^2 d\mathbf{p} \quad (4)$$

Medical anomalies, characterized by high curvature variations  $\kappa = \|\nabla_s \mathbf{n}\|$ , are thus systematically suppressed under this objective.

## 5 Pathway to Medical Utility

### 5.1 Simulation vs. Diagnosis

While our analysis suggests SAM 3D Body is currently unsuited for *diagnostic* reconstruction (where millimeter accuracy is sometimes life-critical), its generalized latent space and robust architecture mean it holds immense potential for *simulation* and offers a promising foundation for fine-tuning to generate domain-specific 3D human body shapes.

Current prompting mechanisms (keypoints) are insufficient to correct this. While we observed from source code of SAM 3D Body only to find it accepts keypoint prompts to resolve *pose* ambiguity, these prompts operate within the constraints of the MHR. If the target shape lies outside the linear span of the shape basis  $B_s$ , no amount of keypoint prompting can force the model to generate it.

This immediate utility can be realized through three primary pathways. Firstly, for High-Volume Avatar Generation, the model’s current fidelity is more than sufficient for applications like mass-casualty Virtual Reality (VR) training or hospital crowd simulation. Secondly, it serves as a robust Procedural Anatomy generator, acting as a clean “base mesh” that can then be deformed by physics-based soft-body solvers [LMR<sup>+</sup>15]. Formally, given a base mesh  $M_0 \sim p_{\text{SAM3D}}(\cdot | I)$  generated from input image  $I$ , deformation parameters  $\phi$  are applied via:

$$M_{\text{deformed}} = \mathcal{D}(M_0, \phi) = M_0 + \sum_{i=1}^{N_v} \mathbf{d}_i(\phi) \quad (5)$$

Finally, and most critically for specialized domains, the model’s powerful generative prior can be effectively leveraged through fine-tuning on limited, private, domain-specific medical datasets (e.g., CT/MRI-derived meshes). This transfer learning paradigm can be expressed as:

$$\theta^* = \arg \min_{\theta} \mathbb{E}_{(I, M) \sim \mathcal{D}_{\text{medical}}} [\mathcal{L}_{\text{geo}}(f_{\theta}(I), M)] + \lambda \|\theta - \theta_{\text{SAM3D}}\|^2 \quad (6)$$

This approach, common and successful in medical foundation model adaptation [WWH<sup>+</sup>25, AAA<sup>+</sup>24, BCK<sup>+</sup>24, MHL<sup>+</sup>24], allows researchers to transfer the model’s generalized knowledge while acquiring the necessary high-fidelity, customized geometric details.

## 6 Future Directions: Medical-in-the-Loop

To bridge the gap from “Artistic” to “Clinical,” we propose the following research directions:

### 6.1 Implicit-Explicit Hybrid Representations

To bypass the parametric bottleneck of MHR, future architectures should integrate 3D Gaussian Splatting [KKLD23] directly into the latent generation process. Approaches like CHROME [DZG<sup>+</sup>25] have demonstrated the efficacy of such hybrid representations for handling occlusion and detail. Rather than relying solely on the mesh  $M(\beta, \theta)$ , we propose a hybrid representation:

$$G = G_{\text{MHR}}(\beta, \theta) + G_{\text{fine}}(\mathcal{G}) \quad (7)$$

where  $G_{\text{MHR}}$  represents the base mesh, and  $G_{\text{fine}}$  is an additive refinement layer parameterized by a set of 3D Gaussians  $\mathcal{G}$ . This allows for adaptive density, allocating more primitives to high-frequency areas (e.g., facial pathology) without increasing the global parameter budget.

## 6.2 Domain-Expert Alignment

We propose that, for a targeted subset of the training data requiring high domain-specific accuracy, annotation be performed exclusively by qualified experts (e.g., board-certified radiologists, anatomists) rather than by generalist annotators. This constitutes a “Medical-in-the-Loop” pipeline. In this refined alignment phase, the reward function must fundamentally shift from the current generalist objective of “perceptual quality” to “pathological fidelity”. This requires careful design of reward functions and ground-truth acquisition, potentially leveraging segmented CT/MRI meshes as the “gold standard” for alignment. Formally, we redefine the preference model from:

$$r_{\text{general}}(G) = \mathbb{E}_{h \sim \mathcal{H}_{\text{general}}} [\text{aesthetic}(G)] \quad (8)$$

to a medically-informed reward:

$$r_{\text{medical}}(G, G_{\text{ref}}) = -\mathcal{L}_{\text{metric}}(G, G_{\text{ref}}) - \lambda_{\text{clinical}} \mathcal{L}_{\text{clinical}}(G, G_{\text{ref}}) \quad (9)$$

where  $G_{\text{ref}}$  is the ground-truth medical reconstruction (e.g., from CT/MRI). Additionally, inspired by the model’s existing separate decoder for hands (‘head\_pose\_hand’), we suggest a hierarchical approach where specific anatomical regions prone to high variance (e.g., spine, abdomen) are handled by specialized expert sub-modules rather than a single global body decoder.

## 6.3 Parametric Injection

Future work may explicitly condition the diffusion or regression process on extended parametric body models that incorporate medical shape parameters, similar to the phenotype-inclusive approach of AnnyBody [BFBS<sup>+</sup>25]. Specifically, by predicting extended shape coefficients ( $\beta_{\text{ext}}$ ) that account for particular conditions such as pregnancy or scoliosis alongside the standard body shape, the model can effectively decouple “body type” from “local geometry”. Consequently, the generative process can be expressed as:

$$G = \mathcal{M}(\beta_{\text{ext}}, \theta) + \Delta(O, \mathbf{c}), \quad (10)$$

where  $\beta_{\text{ext}}$  denotes the extended shape parameters,  $\theta$  represents pose parameters, and  $\Delta(O, \mathbf{c})$  models residual deformations conditioned on observations  $O$  and additional context  $\mathbf{c}$ .

## 7 Conclusion

In this paper, we analyze SAM 3D Body’s consistent failure to reconstruct anthropometric deviations such as pregnancy, scoliosis, and geriatric atrophy. We demonstrate that this is not a capacity limitation but an emergent consequence of optimizing for perceptual quality over geometric fidelity. We identify three mechanisms driving this standardization: MHR’s parametric bottleneck constrains anatomical variance to a low-dimensional linear subspace ( $\mathbb{R}^{45}$  shape,  $\mathbb{R}^{68}$  skeleton) learned from standardized bodies; DINOV3’s semantic invariance and spatial quantization discard medically significant variations as noise; and annotation-based alignment enforces smoothness priors that penalize biological irregularities.

This exemplifies the perception-distortion trade-off in current foundation models, creating a barrier to medical adoption where millimeter-scale features are diagnostically critical. Nevertheless, the model’s robust architecture provides a strong foundation for medical simulation and can be extended via hybrid implicit-explicit representations, targeted fine-tuning on pathological datasets, and Medical-in-the-Loop alignment prioritizing clinical fidelity. Bridging the gap between artistic and clinical 3D reconstruction remains a critical frontier.

## References

[AAA<sup>+</sup>24] Aqilah M Alsaleh, Eid Albalawi, Abdulelah Algosaibi, Salman S Albakheet, and Surbhi Bhatia Khan. Few-shot learning for medical image segmentation using 3d u-net and model-agnostic meta-learning (maml). *Diagnostics*, 14(12):1213, 2024.

[BCK<sup>+</sup>24] Louis Blankemeier, Joseph Paul Cohen, Ashwin Kumar, Dave Van Veen, Syed Jamal Safdar Gardezi, Magdalini Paschali, Zhihong Chen, Jean-Benoit Delbrouck, Eduardo Reis, Cesar Truyts, et al. Merlin: A vision language foundation model for 3d computed tomography. *Research Square*, pages rs-3, 2024.

[BFBS<sup>+</sup>25] Romain Brégier, Guénolé Fiche, Laura Bravo-Sánchez, Thomas Lucas, Matthieu Armando, Philippe Weinzaepfel, Grégory Rogez, and Fabien Baradel. Human mesh modeling for amny body. *arXiv preprint arXiv:2511.03589*, 2025.

[BHVJ25] Mark Boss, Zixuan Huang, Aaryaman Vasishta, and Varun Jampani. Sf3d: Stable fast 3d mesh reconstruction with uv-unwrapping and illumination disentanglement. In *Proceedings of the Computer Vision and Pattern Recognition Conference*, pages 16240–16250, 2025.

[BM18] Yochai Blau and Tomer Michaeli. The perception-distortion tradeoff. In *Proceedings of the IEEE conference on computer vision and pattern recognition*, pages 6228–6237, 2018.

[CLB<sup>+</sup>17] Paul F Christiano, Jan Leike, Tom Brown, Miljan Martic, Shane Legg, and Dario Amodei. Deep reinforcement learning from human preferences. *Advances in neural information processing systems*, 30, 2017.

[CSA<sup>+</sup>25] Yohann Cabon, Lucas Stoffl, Leonid Antsfeld, Gabriela Csurka, Boris Chidlovskii, Jerome Revaud, and Vincent Leroy. Must3r: Multi-view network for stereo 3d reconstruction. In *Proceedings of the Computer Vision and Pattern Recognition Conference*, pages 1050–1060, 2025.

[DZG<sup>+</sup>25] Arindam Dutta, Meng Zheng, Zhongpai Gao, Benjamin Planche, Anwesa Choudhuri, Terrence Chen, Amit K Roy-Chowdhury, and Ziyan Wu. Chrome: Clothed human reconstruction with occlusion-resilience and multiview-consistency from a single image. In *Proceedings of the IEEE/CVF International Conference on Computer Vision*, pages 9124–9135, 2025.

[EHK24] Elizabeth J Enichen, Kimia Heydari, and Joseph C Kvedar. Assessing alternative strategies for measuring metabolic risk. *npj Digital Medicine*, 7(1):360, 2024.

[FOB<sup>+</sup>25] Aaron Ferguson, Ahmed AA Osman, Berta Bescos, Carsten Stoll, Chris Twigg, Christoph Lassner, David Otte, Eric Vignola, Federica Bogo, Igor Santesteban, et al. Mhr: Momentum human rig. *arXiv preprint arXiv:2511.15586*, 2025.

[FSW<sup>+</sup>25] Shuangkang Fang, I Shen, Yufeng Wang, Yi-Hsuan Tsai, Yi Yang, Shuchang Zhou, Wenrui Ding, Takeo Igarashi, Ming-Hsuan Yang, et al. Meshlm: Empowering large language models to progressively understand and generate 3d mesh. In *Proceedings of the IEEE/CVF International Conference on Computer Vision*, pages 14061–14072, 2025.

[GHH<sup>+</sup>24] Ruiqi Gao, Aleksander Holynski, Philipp Henzler, Arthur Brussee, Ricardo Martin-Brualla, Pratul Srinivasan, Jonathan T Barron, and Ben Poole. Cat3d: Create anything in 3d with multi-view diffusion models. *arXiv preprint arXiv:2405.10314*, 2024.

[GLMS<sup>+</sup>23] Manuel Guarnieri Lopez, Katarina L Matthes, Cynthia Sob, Nicole Bender, and Kaspar Staub. Associations between 3d surface scanner derived anthropometric measurements and body composition in a cross-sectional study. *European Journal of Clinical Nutrition*, 77(10):972–981, 2023.

[KKLD23] Bernhard Kerbl, Georgios Kopanas, Thomas Leimkühler, and George Drettakis. 3d gaussian splatting for real-time radiance field rendering. *ACM Trans. Graph.*, 42(4):139–1, 2023.

[LCR24] Vincent Leroy, Yohann Cabon, and Jérôme Revaud. Grounding image matching in 3d with mast3r. In *European Conference on Computer Vision*, pages 71–91. Springer, 2024.

[LMR<sup>+</sup>15] Matthew Loper, Naureen Mahmood, Javier Romero, Gerard Pons-Moll, and Michael J Black. Smpl: a skinned multi-person linear model. *ACM Transactions on Graphics (TOG)*, 34(6):1–16, 2015.

[LYX<sup>+</sup>24] Ziqi Lu, Heng Yang, Danfei Xu, Boyi Li, Boris Ivanovic, Marco Pavone, and Yue Wang. Lora3d: Low-rank self-calibration of 3d geometric foundation models. *arXiv preprint arXiv:2412.07746*, 2024.

[MHL<sup>+</sup>24] Jun Ma, Yuting He, Feifei Li, Lin Han, Chenyu You, and Bo Wang. Segment anything in medical images. *Nature Communications*, 15(1):654, 2024.

[MON<sup>+</sup>19] Lars Mescheder, Michael Oechsle, Michael Niemeyer, Sebastian Nowozin, and Andreas Geiger. Occupancy networks: Learning 3d reconstruction in function space. In *Proceedings of the IEEE/CVF conference on computer vision and pattern recognition*, pages 4460–4470, 2019.

[NSW<sup>+</sup>19] Bennett K Ng, Markus J Sommer, Michael C Wong, Ian Pagano, Yilin Nie, Bo Fan, Samantha Kennedy, Brianna Bourgeois, Nisa Kelly, Yong E Liu, et al. Detailed 3-dimensional body shape features predict body composition, blood metabolites, and functional strength: the shape up! studies. *The American journal of clinical nutrition*, 110(6):1316–1326, 2019.

[OBB20] Ahmed AA Osman, Timo Bolkart, and Michael J Black. Star: Sparse trained articulated human body regressor. In *European Conference on Computer Vision*, pages 598–613. Springer, 2020.

[OBTB22] Ahmed AA Osman, Timo Bolkart, Dimitrios Tzionas, and Michael J Black. Supr: A sparse unified part-based human representation. In *European Conference on Computer Vision*, pages 568–585. Springer, 2022.

[ODM<sup>+</sup>23] Maxime Oquab, Timothée Dariset, Théo Moutakanni, Huy Vo, Marc Szafraniec, Vasil Khalidov, Pierre Fernandez, Daniel Haziza, Francisco Massa, Alaaeldin El-Nouby, et al. Dinov2: Learning robust visual features without supervision. *arXiv preprint arXiv:2304.07193*, 2023.

[PFS<sup>+</sup>19] Jeong Joon Park, Peter Florence, Julian Straub, Richard Newcombe, and Steven Lovegrove. Deepsdf: Learning continuous signed distance functions for shape representation. In *Proceedings of the IEEE/CVF conference on computer vision and pattern recognition*, pages 165–174, 2019.

[PJBM22] Ben Poole, Ajay Jain, Jonathan T Barron, and Ben Mildenhall. Dreamfusion: Text-to-3d using 2d diffusion. *arXiv preprint arXiv:2209.14988*, 2022.

[SMK<sup>+</sup>24] Yawar Siddiqui, Tom Monnier, Filippos Kokkinos, Mahendra Kariya, Yanir Kleiman, Emilien Garreau, Oran Gafni, Natalia Neverova, Andrea Vedaldi, Roman Shapovalov, et al. Meta 3d assetgen: Text-to-mesh generation with high-quality geometry, texture, and pbr materials. *Advances in Neural Information Processing Systems*, 37:9532–9564, 2024.

[SVS<sup>+</sup>25] Oriane Siméoni, Huy V Vo, Maximilian Seitzer, Federico Baldassarre, Maxime Oquab, Cijo Jose, Vasil Khalidov, Marc Szafraniec, Seungeun Yi, Michaël Ramamondjisoa, et al. Dinov3. *arXiv preprint arXiv:2508.10104*, 2025.

[TCB<sup>+</sup>20] Michael Thelwell, Chuang-Yuan Chiu, Alice Bullas, John Hart, Jon Wheat, and Simon Choppin. How shape-based anthropometry can complement traditional anthropometric techniques: a cross-sectional study. *Scientific Reports*, 10(1):12125, 2020.

[TCC<sup>+</sup>24] Jiaxiang Tang, Zhaoxi Chen, Xiaokang Chen, Tengfei Wang, Gang Zeng, and Ziwei Liu. Lgm: Large multi-view gaussian model for high-resolution 3d content creation. In *European Conference on Computer Vision*, pages 1–18. Springer, 2024.

[TCC<sup>+</sup>25] SAM 3D Team, Xingyu Chen, Fu-Jen Chu, et al. Sam 3d: A generative model for visually grounded 3d object reconstruction. *arXiv preprint arXiv:2511.16624*, 2025.

[Ton25] Tonmai. Scoliosis classification dataset. <https://universe.roboflow.com/tonmai-2fwyb/scoliosisclassification>, Jul 2025. Accessed: 2025-11-23.

[WLC<sup>+</sup>24] Shuzhe Wang, Vincent Leroy, Yohann Cabon, Boris Chidlovskii, and Jerome Revaud. Dust3r: Geometric 3d vision made easy. In *Proceedings of the IEEE/CVF Conference on Computer Vision and Pattern Recognition*, pages 20697–20709, 2024.

[WWH<sup>+</sup>25] Junde Wu, Ziyue Wang, Mingxuan Hong, Wei Ji, Huazhu Fu, Yanwu Xu, Min Xu, and Yueming Jin. Medical sam adapter: Adapting segment anything model for medical image segmentation. *Medical image analysis*, 102:103547, 2025.

[WXZ21] Rundi Wu, Chang Xiao, and Changxi Zheng. Deepcad: A deep generative network for computer-aided design models. In *Proceedings of the IEEE/CVF International Conference on Computer Vision*, pages 6772–6782, 2021.

[XDW<sup>+</sup>24] Zhangyang Xiong, Dong Du, Yushuang Wu, Jingqi Dong, Di Kang, Linchao Bao, and Xiaoguang Han. Pifu for the real world: A self-supervised framework to reconstruct dressed human from single-view images. In *International Conference on Computational Visual Media*, pages 3–23. Springer, 2024.

[XLX<sup>+</sup>25] Jianfeng Xiang, Zelong Lv, Sicheng Xu, Yu Deng, Ruicheng Wang, Bowen Zhang, Dong Chen, Xin Tong, and Jiaolong Yang. Structured 3d latents for scalable and versatile 3d generation. In *Proceedings of the Computer Vision and Pattern Recognition Conference*, pages 21469–21480, 2025.

[XZV<sup>+</sup>25] Yan Xia, Xiaowei Zhou, Etienne Vouga, Qixing Huang, and Georgios Pavlakos. Reconstructing humans with a biomechanically accurate skeleton. In *Proceedings of the Computer Vision and Pattern Recognition Conference*, pages 5355–5365, 2025.

[YKP<sup>+</sup>25] Xitong Yang, Devansh Kukreja, Don Pinkus, Anushka Sagar, Taosha Fan, Jinhyung Park, Soyong Shin, Jinkun Cao, Jiawei Liu, Nicolas Ugrinovic, Matt Feiszli, Jitendra Malik, Piotr Dollár, and Kris Kitani. Sam 3d body: Robust full-body human mesh recovery. Technical report, Meta AI Research,

November 2025. Available at <https://ai.meta.com/research/publications/sam-3d-body-robust-full-body-human-mesh-recovery/>.

- [YLZ<sup>+</sup>24] Yifan Yang, Dong Liu, Shuhai Zhang, Zeshuai Deng, Zixiong Huang, and Mingkui Tan. Hilo: Detailed and robust 3d clothed human reconstruction with high-and low-frequency information of parametric models. In *Proceedings of the IEEE/CVF Conference on Computer Vision and Pattern Recognition*, pages 10671–10681, 2024.
- [ZCM<sup>+</sup>25] Lojze Zust, Yohann Cabon, Juliette Marrie, Leonid Antsfeld, Boris Chidlovskii, Jerome Revaud, and Gabriela Csurka. Panst3r: Multi-view consistent panoptic segmentation. *arXiv preprint arXiv:2506.21348*, 2025.
- [ZHH<sup>+</sup>25] Junyi Zhang, Charles Herrmann, Junhwa Hur, Varun Jampani, Trevor Darrell, Forrester Cole, Deqing Sun, and Ming-Hsuan Yang. Monst3r: A simple approach for estimating geometry in the presence of motion. In *ICLR*, 2025.
- [ZLL<sup>+</sup>25] Zibo Zhao, Zeqiang Lai, Qingxiang Lin, Yunfei Zhao, Haolin Liu, Shuhui Yang, Yifei Feng, Mingxin Yang, Sheng Zhang, Xianghui Yang, et al. Hunyuan3d 2.0: Scaling diffusion models for high resolution textured 3d assets generation. *arXiv preprint arXiv:2501.12202*, 2025.
- [ZXY<sup>+</sup>24] Lunjun Zhang, Yuwen Xiong, Ze Yang, Sergio Casas, Rui Hu, and Raquel Urtasun. Copilot4d: Learning unsupervised world models for autonomous driving via discrete diffusion. In *ICLR*, 2024.